

1  
2  
3  
4  
5  
6  
7  
8  
9  
10  
11  
12  
13  
14  
15  
16  
17  
18  
19  
20  
21  
22  
23  
24  
25  
26  
27  
28  
29  
30  
31  
32

## Closed-loop haptic feedback control using a self-sensing soft pneumatic actuator skin

*Harshal A. Sonar<sup>1</sup>, Aaron P. Gerratt<sup>2</sup>, Stéphanie P. Lacour<sup>2</sup>, Jamie Paik<sup>1,\*</sup>*

<sup>1</sup> Reconfigurable Robotics Laboratory, Ecole Polytechnique Fédérale de Lausanne, 1015 Lausanne, Switzerland

<sup>2</sup> Laboratory for Soft Bioelectronic Interfaces, School of Engineering, Center for Neuroprosthetics, EPFL

\*[jamie.paik@epfl.ch](mailto:jamie.paik@epfl.ch)

**Keywords:** Wearable technology, tactile feedback device, liquid metal sensor, strain sensor; soft pneumatic actuators, haptic device.

### **Abstract:**

In this manuscript, we achieve a closed-loop control over haptic feedback, first time for an entirely soft platform. We prototyped a novel self-sensing soft pneumatic actuator (SPA) with soft strain sensors, called SPA-skin, that withstands large multiaxial strains and is capable of high frequency sensing and actuation. To close-loop control the haptic feedback, the platform requires a cohesively integrated system. Our system consists of a stretchable low profile (< 500  $\mu\text{m}$ ) SPA and an ultra-compliant thin-metal film strain sensor that create a novel bidirectional platform for tactile sensing via force-tunable vibratory feedback. With this prototype, we demonstrated control of the actuator shape in real-time up to 100 Hz at output forces up to 1 N, maintained under variable mechanical loadings. We further characterized the SPA-skin platform for its static and dynamic behavior over a range of actuation amplitude and frequencies as well as developed an analytical model of this system to predict the actuator inflation state only using the embedded sensor's resistance. Our SPA-skin is a multifunctional multilayer system that can readily be implemented as a high-speed wearable bidirectional interface for contact sensing and vibrotactile feedback.

## 1 **Objective:**

2

3 Human haptic perception, in addition to visual and auditory feedback, plays a key role in  
4 understanding and exploring our local environment.<sup>[1]</sup> Desktop-scale haptic devices specifically  
5 dedicated for providing tactile stimulation have proven their efficacy in various applications  
6 including medical rehabilitation,<sup>[2]</sup> medical technologies,<sup>[3]</sup> entertainment, and virtual or  
7 augmented reality.<sup>[4]</sup> More compact vibratory haptic actuators have been integrated into system  
8 for human machine interactions such as, car steering wheels, and joysticks;<sup>[5],[6]</sup> however, these  
9 implementations provide limited physical feedback such as in mobile phones and joysticks that  
10 can only modulate its frequency. Furthermore, this frequency modulation is not feedback  
11 controlled.

12

13 For wearable technology to have accurate physical feedback to the wearer, feedback controlled  
14 actuation is needed. As such, the requirements for wearable devices, which include adaptability  
15 and conformability to the body of a human wearer, extends to the haptic technology itself.  
16 Existing haptic technologies, however, do not meet the physical requirements necessary to  
17 achieve these characteristics. Conformable interfaces interacting with human skin should be  
18 made of thin elastic materials that have moduli similar to skin, 0.3 - 2 MPa.<sup>[7]-[11]</sup> This way, the  
19 interface can conform to the body and still operate over a wide frequency range (1 - 400 Hz) and  
20 forces up to 1 N.<sup>[12]</sup> Available tactile feedback devices primarily rely on rigid piezoelectric  
21 elements or electromechanical eccentric mass motors.<sup>[4],[6]</sup> Compliant actuators can be developed  
22 with elastomeric materials such as soft silicones that have elastic moduli similar to human skin.<sup>[7],</sup>  
23 <sup>[8],[11]</sup> The softness and compliance of the soft robotic systems have been useful in many wearable  
24 applications ranging from assistive technologies, medical rehabilitation to entertainment.<sup>[13]-[18]</sup>  
25 Vibro-tactile displays using electro-active polymer (EAP) based soft actuators have tackled many  
26 of the challenges associated with conventional, rigid vibro-tactile devices, but provide limited  
27 wearability as they require high-voltages.<sup>[12],[13]</sup> Soft material-based pneumatic actuators,  
28 composed of elastically inflatable fluidic chambers, have demonstrated their benefits in robotic  
29 applications through large-scale deformation and high compliance, and have potential to be  
30 adapted for wearable haptic applications.<sup>[21]-[28]</sup> The major shortcomings for the pneumatic  
31 powered actuators is the size of the power supply and tube-length limiting the bandwidth for  
32 high-frequency of actuation which need to be separately addressed.

33

34

1 Wearable haptic devices need to ensure that the force imparted on the wearer is consistent with  
2 respect to the perceived performance: this depends on how the interface fits and moves with the  
3 body. The effective tactile feedback also requires accurate and coherent force transfer from the  
4 actuator to the wearer regardless of the external loading or manufacturing variations. This  
5 requires embedded sensing of the actuator state and corresponding corrective measures through  
6 closed-loop control. There has been significant development in entirely soft and stretchable  
7 physical sensors to measure crucial parameters like strain and pressure experienced.<sup>[13], [16], [29]–</sup>  
8 <sup>[32]</sup> Advanced manufacturing technologies like soft 3D printing have combined soft sensing  
9 within soft actuation.<sup>[33]</sup> Such an integration of soft sensing with soft actuation creates possibility  
10 of closed-loop control which is essential to adapt to the external loading conditions suitable for  
11 wearable scenarios. However, no wearable haptic device has demonstrated closed-loop control  
12 capabilities with embedded sensing. It has been particularly difficult to design soft stretchable  
13 sensors, which can perform under high strains and high strain rates needed for state estimation  
14 of high-speed vibratory actuation.

15  
16 We feedback controlled for the first time, an entirely soft haptic platform. We experimented this  
17 on a novel platform composed of a soft sensor integrated soft pneumatic actuator (SPA): SPA-  
18 skin. Its entirely soft design enables flexible, conformal, and distributable interface over a variety  
19 of surfaces. In addition, the integrated sensing and active closed-loop control provide accurate  
20 modulation of actuation amplitude and frequency for rich feedback, independent of an external  
21 loading.

22 The major contributions of this work include:

- 23 1. Active closed-loop control of soft haptic platform independent of the loading conditions.  
24 The closed-loop control compensates for the external disturbance when occurred;  
25 therefore, the produced haptic feedback is consistent and accurate.
- 26 2. Design of a novel haptic platform that is entirely soft, based on a pneumatic actuation and  
27 integrated stretchable liquid metal sensors.
- 28 3. Characterization of SPA-skin for high-fidelity (0-100 Hz) operation and analytical model  
29 to estimate the actuator inflation state using sensor resistance.

30  
31  
32  
33  
34

1

2 **Materials and Methods**3 *SPA-skin design and manufacturing:*

4 The SPA-skin interface, a sensor and actuator laminate, is specifically designed to provide a  
5 consistent vibrotactile feedback under variation of the input parameters: amplitude, vibratory  
6 frequency, and external loading force (**Figure 1**). Amplitude and frequency are the inputs set by  
7 the user-need, while external loading is dictated by the environmental interactions and  
8 disturbance. The sensor-integrated SPA compensates for these three inputs through an active  
9 closed-loop feedback control. Here, a seamlessly integrated stretchable strain sensor measures  
10 the strain experienced upon the actuator inflation by the resistance change. In case of external  
11 loading, the strain value measured is maintained to the set point by actively controlling the input  
12 pressure. We also developed a custom data acquisition platform to enable strain sensing and  
13 actuation control at high-speed (1 kHz) to reliably cover the SPA actuation frequency from 0 to  
14 100 Hz.

15

16 The SPA-skin – a sensor-actuator laminate- is composed of soft silicone elastomers and thin  
17 biphasic metal films, as depicted **Figure 2a**. The actuator layer, SPA, consists of an elastomeric  
18 membrane that can be pneumatically inflated with a positive pressure input.<sup>[34]</sup> This actuator is  
19 fabricated with three thin layers: a middle flexible mask layer (50  $\mu\text{m}$ ) to define the actuator's  
20 shape, sandwiched between two silicone layers, with a total thickness of 500  $\mu\text{m}$ .<sup>[34]</sup> The masking  
21 layer is laser cut to obtain the desired shape and is then laminated onto the bottom silicone layer  
22 to be encapsulated by a thin top silicone layer. The polypropylene mask adheres to the bottom  
23 silicone and ensures that, upon inflation, deformation occurs in the top membrane. The actuator  
24 geometry is governed by the spatial resolution requirement of 20 mm and force requirement of  
25 up to 1 N for sensitivity on the application areas on human back or wrist.<sup>[35], [36]</sup> The actuator area  
26 is 10 mm in diameter and has a 2 mm inlet tube. The sensor layer, an eGaIn filled micro channel  
27 membrane, is prepared with a biphasic (liquid-solid) Gallium-based metallization patterned on a  
28 thin silicone membrane.<sup>[30]</sup> It is then laminated on top of the actuator to complete the soft  
29 actuator-sensor interface. The layout of the strain sensor covers the entire area of the SPA in  
30 order to record changes in strain upon inflation with positive input pressure. The soft sensor-skin  
31 hosts metallic meanders on a 40  $\mu\text{m}$  thick (substrate and encapsulation) on Polydimethylsiloxane  
32 (PDMS) film patterned at the resolution limit of the biphasic metallization technique in order to  
33 maximize the sensor sensitivity. The entire SPA-skin is fabricated using PDMS (Dow Corning  
34 Sylgard 184) because of its low viscoelasticity<sup>[37]</sup> and because multiple layers can be covalently

1 bonded with oxygen plasma treatment. The intentional use of the same material for both the  
2 actuator and the sensor substrate yields a robust monolithic functional skin with embedded  
3 sensing and actuation capabilities. The softness of SPA-skin manufactured matches with that of  
4 the human skin to have a compliant and wearable prototype.

5

## 6 *SPA-skin characterization*

7 The frequency range of somatic perception for human skin varies from 0 - 100 Hz for rapidly  
8 adapting sensor receptors and 100 - 400 Hz Pacinian corpuscles.<sup>[12]</sup> In order to apply a controlled  
9 feedback of the integrated SPA-skin system over such a variety of modulable amplitude and  
10 frequency ranges, an accurate model of the steady state and transient behavior is first needed.  
11 We, therefore, perform static and dynamic characterization of the SPA-skin to obtain all relevant  
12 system parameters necessary for implementing closed-loop control.

13 ***Static characterization*** Despite the addition of extra sensor layer, we observed a minimal  
14 mechanical loading on the SPA with less than 10 % change in the actuator inflation (**Figure 2b**).  
15 The covalent bonding between sensor and actuator layers ensures the conformity of the sensor  
16 layer around the SPA during inflation. This enables the accurate measure of the strain  
17 experienced by the SPA through the soft sensors, even at high strain rates. Upon inflation of the  
18 SPA, the resistance of the soft sensor increases due as the biaxial strain increases. The gauge  
19 factor (GF) observed for the stretchable metallization is approximately unity and independent  
20 of the strain rate [see the supplementary material]. The SPA-skin system exhibited a robust  
21 behaviour, with less than 10 % deviation in the relative change in resistance ( $\Delta R/R$ ) obtained  
22 during high strain rate operation at 20 Hz to a pressure of 25 kPa for a million cycles (**Figure**  
23 **2c**). Such a robustness highlights the ability of the SPA-skin to be used in the wearable  
24 applications over long duration under dynamic operation. The sensors also demonstrate rapid  
25 response times under 1 ms, meeting the demands of the high frequency action for vibrotactile  
26 feedback. During the cyclic test of 1 million cycles at 20 Hz, a 10 % change of resistance per  
27 cycle was observed. This corresponds to an average strain rate of 400 %/s (10 % x 2 x 20 Hz)  
28 experienced by the SPA-skin for a million cycles, with continuous current consumption at  
29 1.25 mA throughout the 14 h of testing period.

30 ***Dynamic characterization*** Our SPA-skin can modulate the actuation amplitude over 100 Hz of  
31 dynamic range of frequencies derived from human mechano-reception capabilities. The SPA-  
32 skin is actuated with an on-off pressure input that is regulated at set amplitudes between,  
33 5 kPa and 30 kPa. The dynamic response shows an increase in the relative change in resistance,  
34  $\Delta R/R_0$ , concomitant to the increase of the actuation pressure at 5 Hz (**Figure 2d**). The inflation

1 and deflation behavior of the sensor-actuator system is repeatable over a range of actuation  
2 frequencies, as seen in the five consecutive cycles shown in **Figure 2c**. The system dynamics  
3 resulting from the material elastic properties and the actuator geometry with  $\phi$  2 mm and tube  
4 length of 300 mm, limit the maximum rate of change in inflation/deflation. This manifests as an  
5 increase in the baseline and decrease in the maximum output as the operational frequency  
6 increases (**Figure 2e**). The cutoff frequency of our SPA-skin design is measured to be 30 Hz,  
7 above which the actuation amplitude is less than 70 % of its maximum value. Although the  
8 vibration amplitude decreases above 30 Hz, it is still measurable and perceivable to the human  
9 skin for the frequencies up to 100 Hz (**Figure 2f**).<sup>[35]</sup> The measurement system can measure the  
10 resistance of sensor dynamically with accuracy of 0.4 % at 1600 samples per second which  
11 enabled recording of 16 samples at 100 Hz. This level of accuracy allowed for measurement of  
12 25 distinct levels for 10 % change in SPA strain.

13

14

15

### 16 *Analytical model and Control strategies*

17 The static and dynamic characteristics of SPA-skin show the integrated system is repeatable and  
18 stable over a range of actuation frequencies and amplitude. The sensor feedback therefore can be  
19 used to actively control the SPA inflation height if the relationship between actuation amplitude  
20 and measured resistance can be developed. It is also important to note that the soft actuators  
21 exhibit complex mechanical behaviour upon inflation due to the hyper-elastic nature of the  
22 silicone materials. Such a behaviour makes it complicated to accurately maintain the actuator  
23 inflation amplitude or output blocked force only with open-loop analytical model without a  
24 feedback sensing mechanism. We utilized the integrated resistive strain sensors to predict the  
25 average strain experienced by actuator and map it to the actuation height. We developed and  
26 experimentally verified an analytical model for the actuator behaviour upon inflation, based on  
27 the results obtained from the integrated resistive sensor-skin, an external inflation height sensor,  
28 and an external pressure sensor (**Figure 3a**). Our model maps the measured resistance change  
29 ( $\Delta R/R_0$ ) from sensor to inflation height ( $h$ ) analytically, based on the actuator inflation geometry  
30 and biaxial deformation of material upon inflation. In the first stage we developed geometrical  
31 mapping function for the measured strain for a given inflation height (**Figure 3a**). As the strain  
32 experienced by the sensor meanders is equibiaxial, we then map it to corresponding change in  
33 resistance value resulting from the actuator inflation.

34

1 Assuming a Poisson's ratio ( $\nu$ ) of 0.5 for PDMS and an isotropic nature of the soft material, we  
 2 can assume equibiaxial stress in the actuator membrane upon inflation. Also, the effect of  
 3 reduction in the remaining dimensions ( $-\varepsilon'$ ) for applied strain ( $\varepsilon$ ) in one dimension for a given  
 4 Poisson's ratio is:

$$(1 - \varepsilon') = (1 + \varepsilon)^{-\nu} \quad (1)$$

6 Therefore, the change in dimensions of a single meander channel with length ( $l_0$ ), width ( $w_0$ ),  
 7 and thickness ( $t_0$ ) from equibiaxial strain upon inflation ( $\varepsilon = \varepsilon_l = \varepsilon_w$ ) can be given as:

$$l = l_0 + \Delta l_l - \Delta l_w = l_0 (1 + \varepsilon_l - \varepsilon'_w) = l_0 [(1 + \varepsilon)^{-\nu} + \varepsilon];$$

$$w = w_0 - \Delta w_l + \Delta w_w = w_0 (1 - \varepsilon'_l + \varepsilon_w) = w_0 [(1 + \varepsilon)^{-\nu} + \varepsilon];$$

$$t = t_0 - \Delta t_l - \Delta t_w = t_0 (1 - \varepsilon'_l + 1 - \varepsilon'_w - 1) = t_0 [2(1 + \varepsilon)^{-\nu} - 1] \quad (2)$$

11 Where,  $\Delta l_{l/w}$ ,  $\Delta w_{l/w}$  and  $\Delta t_{l/w}$  are changes in length, width and height of the soft material due  
 12 to strain in the direction of length/width ( $l/w$ ), respectively.

13 Hence, the change in resistance of the biphasic metal encapsulated within the silicone membranes  
 14 can be given as:

$$\frac{R}{R_0} = \frac{l/l_0}{(w/w_0)(t/t_0)} = \frac{1}{2(1+\varepsilon)^{-\nu}-1} \quad (3)$$

16 Furthermore, the correlation between uniaxial strain and actuator inflation height can be  
 17 formulated using the volumetric change in the actuator and spatial distribution of sensor  
 18 meanders on the actuator. The actuator of diameter ( $d$ ) inflated to height ( $h$ ) takes the  
 19 approximate shape of a scooped sphere with a variable radius ( $r$ ) (**Figure 3a, b**). The radius  
 20 decreases from infinity to 5 mm as actuator inflates from 0 mm to 5 mm height. The average  
 21 uniaxial strain in a single meander during inflation to height can be described as:

$$\varepsilon = \frac{l-l_0}{l_0} = \frac{\sin^{-1} \frac{x}{r}}{\frac{x}{r}} - 1 \quad (4)$$

23 Where,  $x$  is the actuator radius,  $l$  is the final length,  $l_0$  is initial length, and  $r = \sqrt{x^2 + (r-h)^2}$ .

24 The sensor meander pattern consists of 18 parallel lines equally distribute along the surface of  
 25 the actuator membrane. The  $i^{th}$  stripe of the sensor channel is distance ( $d_i$ ) from center of the  
 26 actuator and during inflation reaches height ( $h_i$ ):

$$h_i = h_{max} - r + \sqrt{r^2 - d_i^2} \quad (5)$$

28 From Equations 3 and 4, the average strain experienced by all the sensor meanders on the  
 29 actuator surface is given as:

$$\varepsilon_{\text{avg}} = \sum_{i=1}^n \frac{\varepsilon_i}{n} = \frac{1}{n} \sum_{i=1}^n \left\{ \frac{\sin^{-1} \frac{x}{r_i}}{\frac{x}{r_i}} - 1 \right\} \approx \frac{\Delta R}{R} \quad (6)$$

2 Where, the GF is 1.<sup>[30]</sup>

3 Hence, to deduce the inflation height ( $h$ ) by measuring change in resistance ( $\Delta R/R_0$ ) an explicit  
 4 mapping from  $\Delta R/R_0 \rightarrow h$  is necessary. However, it is impossible to obtain, as Equation 2 is a  
 5 coupled equation. Therefore, a piecewise polynomial curve fit is obtained for the inverse  
 6 mapping of Equation 2 (**Figure 3c**):

$$7 \quad h = 49800 \left( \frac{\Delta R}{R_0} \right)^3 - 2890 \left( \frac{\Delta R}{R_0} \right)^2 + 74.6 \left( \frac{\Delta R}{R_0} \right) + 0.109 \text{ for } 0 < \left( \frac{\Delta R}{R_0} \right) < 0.025$$

$$8 \quad h = 33 \left( \frac{\Delta R}{R_0} \right)^3 - 31 \left( \frac{\Delta R}{R_0} \right)^2 + 16 \left( \frac{\Delta R}{R_0} \right) + 0.63 \text{ for } 0.025 < \left( \frac{\Delta R}{R_0} \right) < 0.4$$

9 with Error Norm= 0.0079.

10

11

## 12 **Results**

### 13 *Experimental setup*

14 High-speed actuation of SPA-skin demands a test setup that provides a high data rate resistance  
 15 measurement and a low settling time pressure regulation. We required at least 1000  
 16 samples/second of sensor resistance values in order to ensure reliable and accurate estimation of  
 17 actuator state, as a digital control system needs at least 8-10 times more samples than the actual  
 18 operational frequency of the system (100 Hz for SPA-skin). We developed a custom 16-bit high-  
 19 speed data acquisition system with a low on-resistance multiplexer, A/DC (ADS8517, TI, USA)  
 20 and an Arduino microcontroller board that measured the sensor resistance at 1600 Hz per channel  
 21 with 0.4% accuracy (**Figure 3a**). The low resistance multiplexer reduced the effect of extra  
 22 resistance added in the sensor resistance measurement. It was also necessary to have a pressure  
 23 regulator that can react within 10 ms to be able to control the SPA-skin at 100 Hz of vibratory  
 24 output. In practice, we obtained settling time of 20 ms with a piezo-actuator drive pressure for  
 25 maximum pressure change from 0 to 100 kPa that allowed us to control SPA-skin up to 50 Hz.  
 26 The Arduino microcontroller also directed the control commands to this piezo-pressure regulator  
 27 to achieve the desired set point. The test setup is also equipped with an integrated pressure sensor  
 28 (001BGAA5, Honeywell) and a laser interferometer (HG-C1030, Panasonic) to measure the SPA  
 29 pressure and the inflation height, respectively. There is a micro-meter placed vertically and  
 30 connected to a high precision 3D force sensor (Nano 17, ATI industrial automation, USA) for



1 applying a controlled blocked force externally to simulate disturbances.[supplementary **Figure**  
2 **S3c**].

3

#### 4 *Model validation*

5 Our test setup enabled measurement of inflation height, input pressure and strain sensor  
6 resistance to process the data for validation of the analytical model developed in previous section.  
7 We measured the maximum height ( $h_{max}$ ) during inflation at the given pressure with an external  
8 laser displacement sensor and recording the sensor response as depicted in **Figure 3b**. We  
9 inflated SPA-skin at various input pressure and took images for fitting a curve of radius 'r' and  
10 while simultaneously measuring the observed inflation height ( $h$ ). The experimental values of  
11 curved fitted radii with the scooped sphere approximation for given inflation height matches  
12 closely with the expected geometrical model (**Figure 3b**). Afterwards, we derived the average  
13 strain values from the Equation 5 and the external height sensor reading. Assuming the GF of 1  
14 we obtained the analytical model plot of expected resistance change ( $\frac{\Delta R}{R}$ ) for given inflation  
15 height in **Figure 3c**. The subsequent experimental measurements shows the resistance change  
16 over inflation height of SPA-skin for three different samples are well in agreement with the  
17 analytical model (**Figure 3c**) [and supplementary **Figure S2**]. This confirmed the integrated  
18 strain sensor could effectively be used to measure the actuator inflation height, eliminating the  
19 dependency of actuator performance on the manufacturing variations and input pressure. Next,  
20 we developed a strain controller to have the strain sensor for active closed loop control.

21

#### 22 *Active control of the force exerted by the SPA-skin*

23 A coherent and responsive haptic feedback from deformable soft interfaces relies on explicit  
24 control of the actuation force and frequency, regardless of the loading conditions. If not, the  
25 wearer will feel unstable feedback depending on how the device is positioned. Hence, we  
26 demonstrated the closed-loop capabilities to actively adapt for the changes in the loading and  
27 provide a coherent tactile feedback. We designed a setup which uses a 1 cm<sup>3</sup> cube of Ecoflex 30  
28 silicone <sup>[8]</sup> to simulate contact with the human skin, placed over the SPA-skin (**Figure 4a**).  
29 Ecoflex 30 is selected as its compressive behavior is comparable with that of human skin.<sup>[38]</sup>  
30 We have the relationship between the measured resistance and the biaxial strain on the system  
31 from the analytical model. The biaxial strain maintained under uniform soft loading will provide  
32 compensation for the added pressure through increase in the input pressure.

33

1 A PID controller is developed with desired resistance as setpoint to control the input pressure  
2 and eventually the inflation amplitude to demonstrate the closed-loop control capabilities of the  
3 SPA-skin. During free, unloaded operation, the control loop easily achieved the arbitrary strain  
4 set points (**Figure 4b**). Additionally when external forces were introduced, the system continues  
5 to converge to the set point inflation, regardless of the pre-load (**Figure 4c**). The feedback from  
6 the embedded strain sensors guarantees the desired actuation, even when the external loading is  
7 an order of magnitude higher than the desired blocked-force produced by the SPA-skin  
8 (**Figure 4d**). Eventually, as the loading increases, the system's mechanical inertia increases,  
9 which leads to an increase in the overshoot in the control (**Figure 4c**). We tuned the PID gains  
10 conservatively to cover this fact and compensate for the overshoot, while degrading a little on  
11 the system settling time.

12

13

14

## 15 **Conclusion**

16 For an effective wearable technology, we require an accurate understanding of the physical  
17 interactions between the device and the wearer's perception. We engineered a closed-loop  
18 control of an entirely soft wearable haptic platform over a wide range of vibrotactile feedback.

19 The soft material based device design provided inherent safety much needed for human  
20 interaction as well as compliance matching with human skin to provide natural wearability.

21 We prototyped a soft monolithic sensor integrated SPA with embedded sensing and actuation  
22 capabilities, and with soft sensors that have no mechanical loading impact on the actuator. Use  
23 of SPAs provided high actuation force, wide range of actuation frequency, simple design for  
24 iteration and a highly customizable thin platform as opposed to the traditionally available rigid  
25 vibration motors. The SPA-skin produced forces up to 1 N with controllability of 0.05 N, and  
26 actuation dynamics of up to 100 Hz with controllability of 0.1 Hz; these are essential for  
27 providing a wide range of proprioceptive feedback to the wearer. The system characterization  
28 of SPA-skin under continuous actuation and sensing showed robust and repeatable behavior over  
29 1 million cycles thereby promising compatibility with "real life" wearable applications. We  
30 further demonstrated closed-loop control capabilities of this SPA-skin system at 15 Hz sinusoidal  
31 vibration at 1 kHz control speed. The closed-loop controller, based on an analytical model of the  
32 system, uses the sensor resistance to control the average strain of the actuator and allow for  
33 generating uniform output force under different loading conditions. This allowed the wearer to  
34 feel a consistent feedback independent of the wearing conditions. Furthermore, the bidirectional

1 operations of the SPA-skin platform offer a wearable system that can not only be used for haptic  
2 feedback but also for quantification of human proprioceptive capabilities over range of  
3 frequencies. This makes SPA-skin a promising solution for applications demanding more  
4 intuitive and comprehensive tactile interactions. Specifically SPA skin allows user studies can  
5 benefit from this quantitative measurement of feedback through integrated soft sensing to match  
6 with user's qualitative responses over tactile feedback.

7

8 << talk about SPA-skin Array >>

9

10

11

## 12 **Acknowledgement**

13 The authors would like to thank the Swiss National Centre of Competence in Research (NCCR)  
14 in Robotics, the European Research Project Proof of Concept grant (SoWe), and the Bertarelli  
15 Foundation.

16

17

18

19

20

21

22

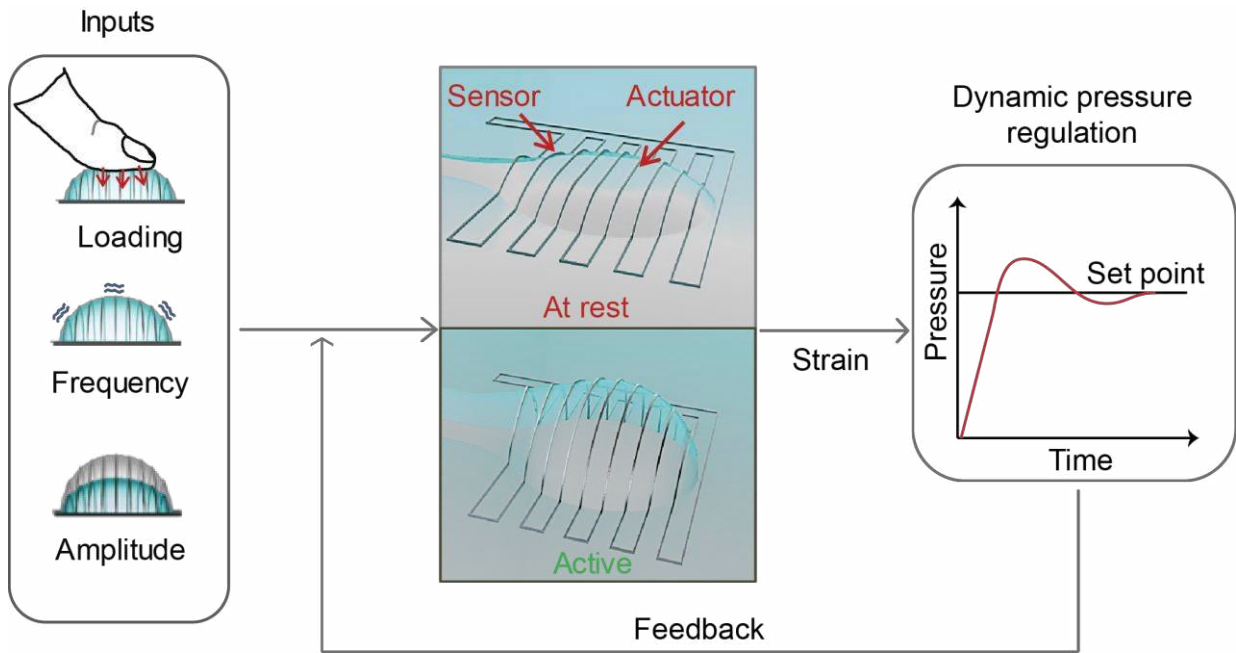
23

## 24 **References:**

- 25 [1] J. Minogue and M. G. Jones, "Haptics in Education: Exploring an Untapped Sensory  
26 Modality," *Rev. Educ. Res.*, vol. 76, no. 3, pp. 317–348, Jan. 2006.
- 27 [2] R. Sigrist, G. Rauter, R. Riener, and P. Wolf, "Augmented visual, auditory, haptic, and  
28 multimodal feedback in motor learning: A review," *Psychon. Bull. Rev.*, vol. 20, no. 1, pp.  
29 21–53, Feb. 2013.
- 30 [3] E. P. Westebring-van der Putten, R. H. M. Goossens, J. J. Jakimowicz, and J. Dankelman,  
31 "Haptics in minimally invasive surgery--a review," *Minim. Invasive Ther. Allied Technol.*  
32 *MITAT Off. J. Soc. Minim. Invasive Ther.*, vol. 17, no. 1, pp. 3–16, 2008.
- 33 [4] A. U. Alahakone and S. M. N. A. Senanayake, "Vibrotactile feedback systems: Current  
34 trends in rehabilitation, sports and information display," in *2009 IEEE/ASME*  
35 *International Conference on Advanced Intelligent Mechatronics*, 2009, pp. 1148–1153.

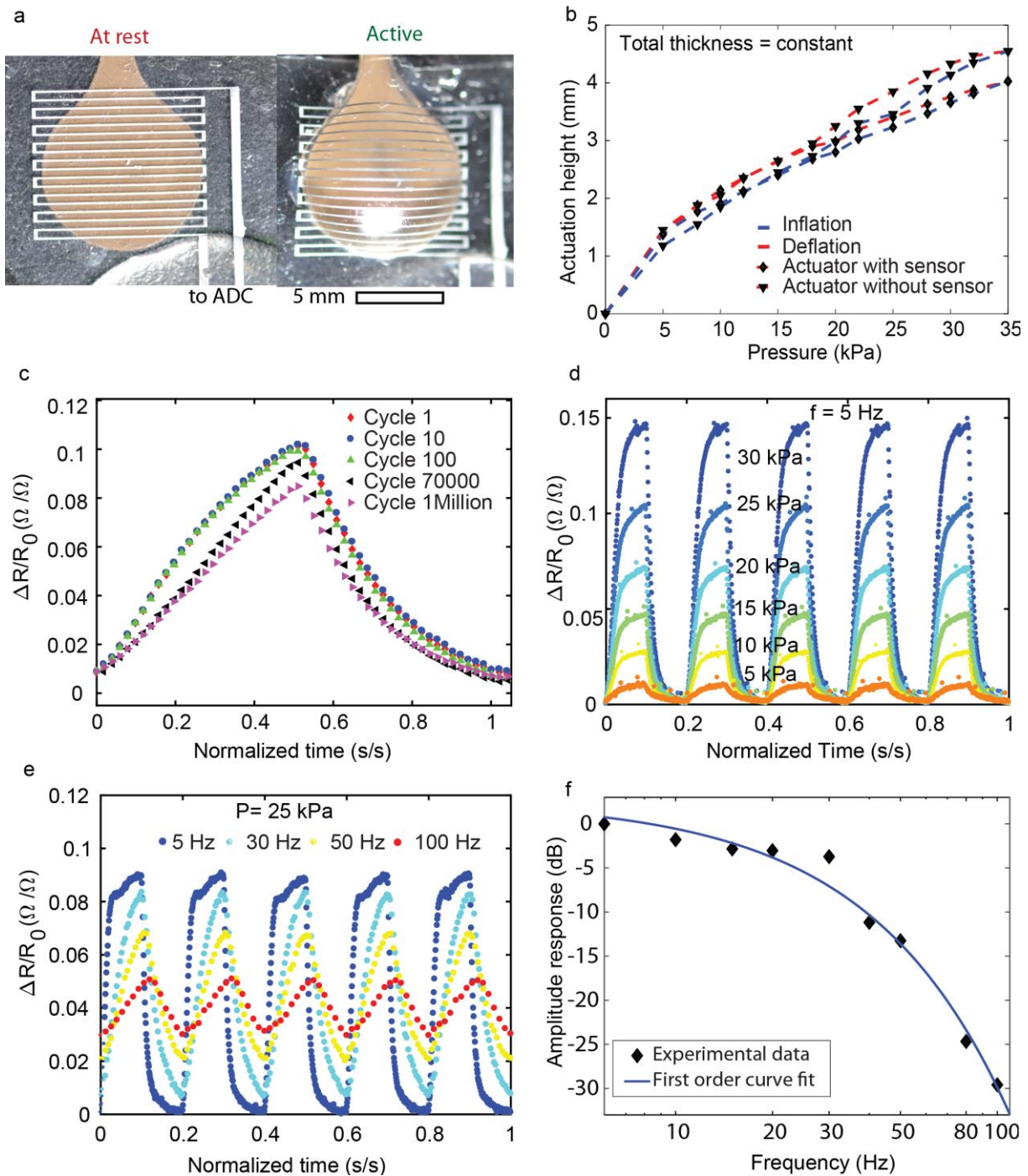
- 1 [5] Vincent Hayward, Oliver R. Astley, Manuel Cruz-Hernandez, Danny Grant, and Gabriel  
2 Robles-De-La-Torre, "Haptic interfaces and devices," *Sens. Rev.*, vol. 24, no. 1, pp. 16–29,  
3 Mar. 2004.
- 4 [6] "Vibration Motors", *Precision Microdrives*. [Online]. Available:  
5 <https://www.precisionmicrodrives.com/vibration-motors>.
- 6 [7] I. D. Johnston, D. K. McCluskey, C. K. L. Tan, and M. C. Tracey, "Mechanical  
7 characterization of bulk Sylgard 184 for microfluidics and microengineering," *J.*  
8 *Micromechanics Microengineering*, vol. 24, no. 3, p. 035017, 2014.
- 9 [8] "Ecoflex® 00-30 Product Information," *Smooth-On, Inc.* [Online]. Available:  
10 <https://www.smooth-on.com/products/ecoflex-00-30/>.
- 11 [9] S. Diridollou *et al.*, "In vivo model of the mechanical properties of the human skin under  
12 suction," *Skin Res. Technol.*, vol. 6, no. 4, pp. 214–221.
- 13 [10] J. C. Case, E. L. White, and R. K. Kramer, "Soft Material Characterization for Robotic  
14 Applications," *Soft Robot.*, vol. 2, no. 2, pp. 80–87, Jun. 2015.
- 15 [11] G. Alici, "Softer is Harder: What Differentiates Soft Robotics from Hard Robotics?," *MRS*  
16 *Adv.*, vol. 3, no. 28, pp. 1557–1568, ed 2018.
- 17 [12] S. Choi and K. J. Kuchenbecker, "Vibrotactile Display: Perception, Technology, and  
18 Applications," *Proc. IEEE*, vol. 101, no. 9, pp. 2093–2104, Sep. 2013.
- 19 [13] S. Bauer, S. Bauer-Gogonea, I. Graz, M. Kaltenbrunner, C. Keplinger, and R. Schwödauer,  
20 "25th Anniversary Article: A Soft Future: From Robots and Sensor Skin to Energy  
21 Harvesters," *Adv. Mater.*, vol. 26, no. 1, pp. 149–162, Jan. 2014.
- 22 [14] S. Yun, B. B. Kang, and K. Cho, "Exo-Glove PM: An Easily Customizable Modularized  
23 Pneumatic Assistive Glove," *IEEE Robot. Autom. Lett.*, vol. 2, no. 3, pp. 1725–1732, Jul.  
24 2017.
- 25 [15] E. W. Hawkes, L. H. Blumenschein, J. D. Greer, and A. M. Okamura, "A soft robot that  
26 navigates its environment through growth," *Sci. Robot.*, vol. 2, no. 8, p. ean3028, Jul.  
27 2017.
- 28 [16] P. Polygerinos *et al.*, "Soft Robotics: Review of Fluid-Driven Intrinsically Soft Devices;  
29 Manufacturing, Sensing, Control, and Applications in Human-Robot Interaction," *Adv.*  
30 *Eng. Mater.*, vol. 19, no. 12, p. 1700016, Dec. 2017.
- 31 [17] M. Cianchetti, C. Laschi, A. Menciassi, and P. Dario, "Biomedical applications of soft  
32 robotics," *Nat. Rev. Mater.*, vol. 3, no. 6, p. 143, Jun. 2018.
- 33 [18] N. Agharese *et al.*, "HapWRAP: Soft Growing Wearable Haptic Device," in *2018 IEEE*  
34 *International Conference on Robotics and Automation (ICRA)*, 2018, pp. 1–5.
- 35 [19] H. Phung *et al.*, "Tactile display with rigid coupling based on soft actuator," *Meccanica*,  
36 vol. 50, no. 11, pp. 2825–2837, Nov. 2015.
- 37 [20] A. Murette, A. Poulin, N. Besse, S. Rosset, D. Briand, and H. Shea, "Flexible Zinc–Tin Oxide  
38 Thin Film Transistors Operating at 1 kV for Integrated Switching of Dielectric Elastomer  
39 Actuators Arrays," *Adv. Mater.*, vol. 29, no. 30, p. 1700880, Aug. 2017.
- 40 [21] P. Moseley, J. M. Florez, H. A. Sonar, G. Agarwal, W. Curtin, and J. Paik, "Modeling,  
41 Design, and Development of Soft Pneumatic Actuators with Finite Element Method,"  
42 *Adv. Eng. Mater.*, vol. 18, no. 6, pp. 978–988, Jun. 2016.
- 43 [22] G. Agarwal, N. Besuchet, B. Audergon, and J. Paik, "Stretchable Materials for Robust Soft  
44 Actuators towards Assistive Wearable Devices," *Sci. Rep.*, vol. 6, Sep. 2016.
- 45 [23] R. V. Martinez, A. C. Glavan, C. Keplinger, A. I. Oyetibo, and G. M. Whitesides, "Soft  
46 Actuators and Robots that Are Resistant to Mechanical Damage," *Adv. Funct. Mater.*, vol.  
47 24, no. 20, pp. 3003–3010, May 2014.

- 1 [24] B. Mosadegh *et al.*, “Pneumatic Networks for Soft Robotics that Actuate Rapidly,” *Adv.*  
2 *Funct. Mater.*, vol. 24, no. 15, pp. 2163–2170, Apr. 2014.
- 3 [25] M. A. Robertson and J. Paik, “New soft robots really suck: Vacuum-powered systems  
4 empower diverse capabilities,” *Sci. Robot.*, vol. 2, no. 9, p. ean6357, Aug. 2017.
- 5 [26] C. Larson *et al.*, “Highly stretchable electroluminescent skin for optical signaling and  
6 tactile sensing,” *Science*, vol. 351, no. 6277, pp. 1071–1074, Mar. 2016.
- 7 [27] J. Shintake, H. Sonar, E. Piskarev, J. Paik, and D. Floreano, “Soft pneumatic gelatin  
8 actuator for edible robotics,” in *2017 IEEE/RSJ International Conference on Intelligent*  
9 *Robots and Systems (IROS)*, 2017, pp. 6221–6226.
- 10 [28] D. Rus and M. T. Tolley, “Design, fabrication and control of soft robots,” *Nature*, vol. 521,  
11 no. 7553, pp. 467–475, May 2015.
- 12 [29] T. Q. Trung and N. Lee, “Flexible and Stretchable Physical Sensor Integrated Platforms for  
13 Wearable Human-Activity Monitoring and Personal Healthcare,” *Adv. Mater.*, 2016.
- 14 [30] A. Hirsch, H. O. Michaud, A. P. Gerratt, S. de Mulatier, and S. P. Lacour, “Intrinsically  
15 Stretchable Biphasic (Solid–Liquid) Thin Metal Films,” *Adv. Mater.*, vol. 28, no. 22, pp.  
16 4507–4512, Jun. 2016.
- 17 [31] S. Nam *et al.*, “A Robust Soft Lens for Tunable Camera Application Using Dielectric  
18 Elastomer Actuators,” *Soft Robot.*, Aug. 2018.
- 19 [32] H. Mößinger, H. Haus, M. Kauer, and H. F. Schlaak, “Tactile feedback to the palm using  
20 arbitrarily shaped DEA,” presented at the Electroactive Polymer Actuators and Devices  
21 (EAPAD) 2014, 2014, vol. 9056, p. 90563C.
- 22 [33] R. L. Truby *et al.*, “Soft Somatosensitive Actuators via Embedded 3D Printing,” *Adv.*  
23 *Mater.*, 2018.
- 24 [34] H. A. Sonar and J. Paik, “Soft Pneumatic Actuator Skin with Piezoelectric Sensors for  
25 Vibrotactile Feedback,” *Front. Robot. AI*, vol. 2, 2016.
- 26 [35] B. J. P. Mortimer, G. A. Zets, and R. W. Cholewiak, “Vibrotactile transduction and  
27 transducers,” *J. Acoust. Soc. Am.*, vol. 121, no. 5, pp. 2970–2977, May 2007.
- 28 [36] K. A. Kaczmarek, J. G. Webster, P. Bach-y-Rita, and W. J. Tompkins, “Electrotactile and  
29 vibrotactile displays for sensory substitution systems,” *IEEE Trans. Biomed. Eng.*, vol. 38,  
30 no. 1, pp. 1–16, Jan. 1991.
- 31 [37] F. Schneider, U. Wallrabe, T. Fellner, and J. Wilde, “Mechanical properties of silicones for  
32 MEMS,” *J. Micromechanics Microengineering Struct. Devices Syst.*, vol. 18, no. 6, 2008.
- 33 [38] J. L. Sparks *et al.*, “Use of silicone materials to simulate tissue biomechanics as related to  
34 deep tissue injury,” *Adv. Skin Wound Care*, vol. 28, no. 2, pp. 59–68, Feb. 2015.
- 35

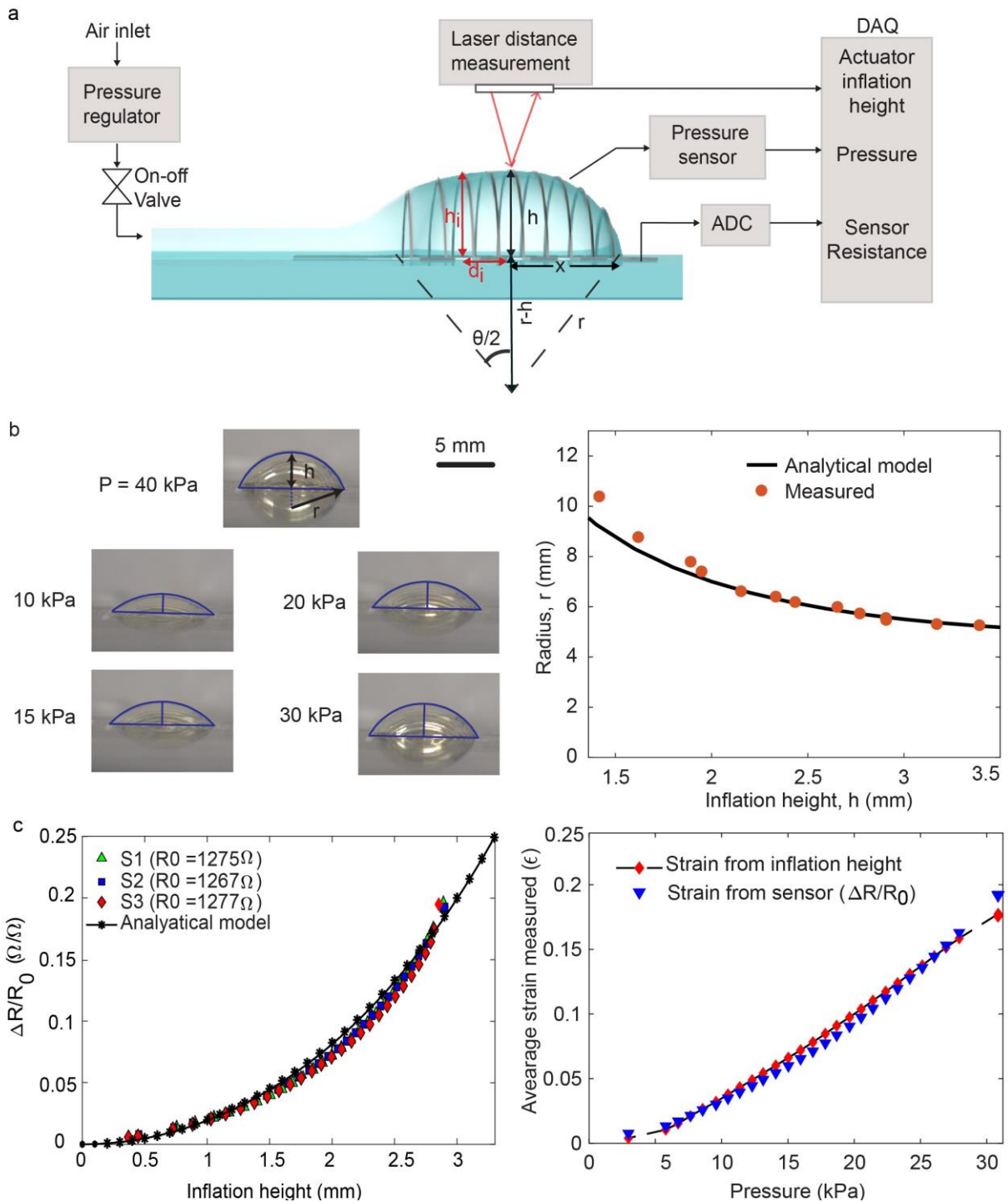


1

**Figure 1. Feedback control loop of soft haptic system.** The SPA-skin provides a highly conformal interface. A strain sensor of stretchable metallization can be used as the input to a feedback loop used to control the actuator inflation and exerted force. High-speed data acquisition allows strain sensing and actuation over a range of actuation frequencies from 0 to 100 Hz.



1  
 2 **Figure 2. Characterization of SPA-Skin.** (a) An SPA-skin prototype before and during  
 3 inflation. (b) Actuators of the same thickness with and without laminated sensors show little  
 4 change in performance. (c) Sensor performance over a million cycles. (d) SPA-skin response for  
 5 variation input pressure set points from 5 kPa to 30 kPa at 5 Hz. (e) SPA-skin response for  
 6 variation of actuation frequency from 5 Hz to 100 Hz at 25 kPa pressure set point. (f) SPA-skin  
 7 amplitude response for variation in actuation frequency.



1  
 2 **Figure 3. Experimental setup and model.** (a) Experimental setup for validating the sensor embedded  
 3 SPA model upon actuation, overlaying the geometrical parameters used in the analytical model. (b) Images  
 4 showing the SPA inflation over a range of actuation pressures used to measure the inflation radius ( $r$ ) and  
 5 the inflation height ( $h$ ) for geometrical model validation. The measured inflation radius is compared with  
 6 the geometric model assuming the SPA inflation geometry as a part of a scooped sphere.. (c) Average  
 7 measured and computed strains for given inflation heights. (d) Average strain as a function of input  
 8 pressure (red dots: model, blue dots: experimental strain measured by the resistive sensor).



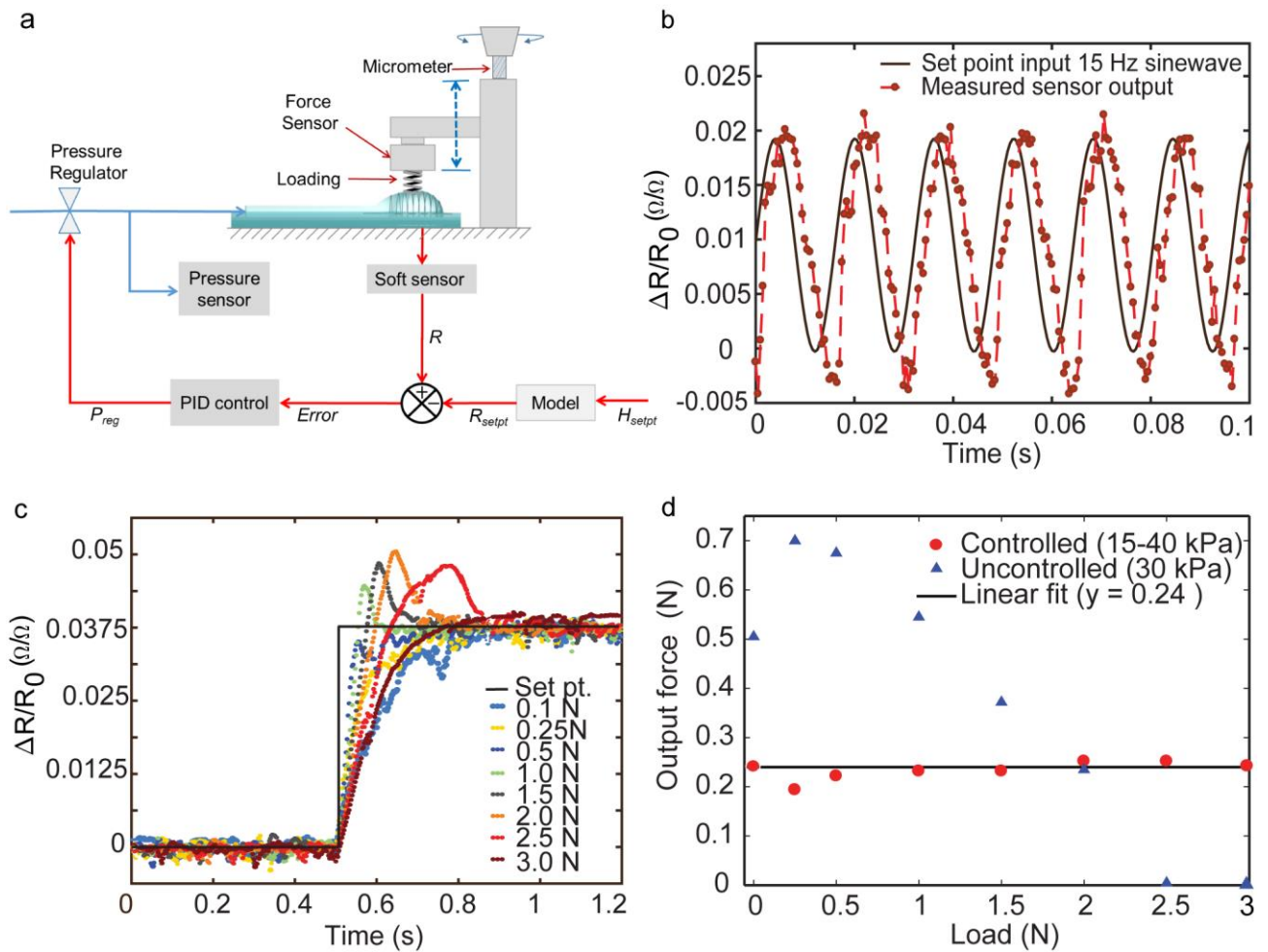


**Figure 4. Testbed for active closed-loop control.** (a) Control flow diagram of the SPA-skin with a soft, skin-like material placed between the actuator and an external force sensor, simulating external loading of the sensor against skin. Strain is controlled using PID controller regulate SPA pressure. External pressure sensor limits the maximum input pressure for safe operation. A Vernier scale controls the displacement, and therefore blocked force. (b) Controller tracking a sinusoidal perturbation of set point input at 15 Hz. (c) Controller performance under eight different loading conditions. The controller has a damped response at 3 N as the pressure required to achieve the set point exceeds the 40 kPa pressure controller safety limit. (d) Effect of loading on the SPA-skin performance when controlled using a pressure sensor and when using an integrated strain sensor to achieve a 0.25 N blocked force set point.

1  
2  
3  
4  
5  
6  
7  
8  
9  
10  
11  
12  
13  
14